Measurement 49 (2014) 60–67

Contents lists available at ScienceDirect

Measurement

journal homepage: www.elsevier.com/locate/measurement

Measurement and statistical analysis toward reproducibility validation of AZ4562 cylindrical microlenses obtained by reflow

Marino de Jesus Maciel, Rui Pedro Rocha, João Paulo Carmo *, José Higino Correia

University of Minho, Dept. of Industrial Electronics, Campus Azurem, 4800-058 Guimaraes, Portugal

ARTICLE INFO

Article history:
Received 11 August 2013
Received in revised form 16 October 2013
Accepted 28 November 2013
Available online 3 December 2013

Keywords:
Measurement
Statistic analysis
Reproducibility validation
Microlenses fabrication

ABSTRACT

This paper presents the statistical analysis applied into the shape of microlenses (MLs) for validating the high-reproducibility feature of their fabrication process. The MLs were fabricated with the AZ4562 photoresist, using photolithography and thermal reflow processes. Two types of MLs arrays were produced for statistical analysis purposes: the first with a cross-sectional diameter of 24 μm and the second with a cross-sectional diameter of 30 μm, and both with 5 μm spacing between MLs. In the case of 24 μm diameter arrays, the measurements showed a mean difference in diameter of 2.78 μm with a standard deviation (SD) of 0.22 μm (e.g., 2.78 ± 0.22 μm of SD) before the reflow, and 2.34 ± 0.35 μm of SD after the reflow. For the same arrays, the mean difference in height obtained was, comparatively to the 5.06 μm expected, 0.76 ± 0.10 μm of SD before the reflow and 1.91 ± 0.15 μm of SD after the reflow, respectively. A mean difference in diameter of 2.64 ± 0.41 μm of SD before the reflow, and 1.87 ± 0.34 μm of SD after the reflow was obtained for 30 μm diameter MLs arrays. For these MLs, a mean difference in height of 0.71 ± 0.12 μm of SD before the reflow and 2.24 ± 0.24 μm of SD after the thermal reflow was obtained, in comparison to the 5.06 μm of height expected to obtain. These results validate the requirement for reproducibility and opens good perspectives for applying this fabrication process on high-volume production of MLs arrays.

1. Introduction

Micro-optical elements are essential parts in different applications, including optical fiber-based instruments [1], optical inspection with micrometer precision [2], communications, image sensors, biomedical devices [3,4], confocal microscopy [5], and in advanced optical products [6]. Microlenses (MLs) are an example of those micro-optical elements usually integrated with optical systems for collimation and focusing. Additionally, MLs are an attractive alternative for applications where miniaturization, low cost and alignment simplicity are primordial [4]. Examples of these applications include image sensors, biomedical instruments, microsystems and lab-on-a-chip systems [3,4]. The MLs can be fabricated using different methods found in literature [7–10] such as e-beam lithography, hot embossing, reactive ion etching, ion diffusion, photoresist reflow method, LIGA. The most used fabrication process is the thermal reflow one due to its simplicity, rapidity and low cost. Furthermore, only lithography and heating processes are required [11,12]. Basically, a photoresist (PR) material, like AZ4562, is patterned after a lithography process. Then, the thermal reflow is applied to PR and, due to surface tension phenomena, the material acquire the lens profile [13,14]. In this context, this paper presents a reproducibility analysis applied to MLs fabrication with thermal reflow process. Only cylindrical MLs were fabricated and tested. Photolithography was used to pattern two types of strips, according to the designed photo-mask: one with a diameter of 24 μm and other with

* Corresponding author. Tel.: + 351 253510190; fax: + 351 253510189.
E-mail address: jcarmo@dei.uminho.pt (J.P. Carmo).

0263-2241/$ - see front matter © 2013 Elsevier Ltd. All rights reserved.
http://dx.doi.org/10.1016/j.measurement.2013.11.056

30 μm, spacing 5 μm. After this phase, a statistical analysis was done before the reflow. Then, it was analyzed other parameters, e.g., the cross-sectional diameter, the height and the distance between adjacent MLs. Another set of MLs were produced with the same parameters and at the same time, the thermal reflow was also applied. For these MLs a post thermal reflow statistical analysis was performed. The different MLs were fabricated on different occasions in order to allow the statistical analysis to be statistically significant. This last issue is important to take reliable conclusions about the fully reproducibility of this fabrication process.

Cross-sectional diameter, height and distance between adjacent strips were the parameters chosen for reproducibility study of the photolithography process. The aim of this statistical study is to conclude the lithography process's capacity in convert the two-dimensional photo mask design in a three-dimensional structure with a thickness, length and height. After applied the thermal reflow, the same parameters were chosen to statistically study the thermal reflow process in cylindrical MLs. Other parameters could be chosen to validate the reproducibility of the MLs fabrication, like curvature deviation, off-axis deviation, point-spread function (PSF) [9,15]. However, these parameters chosen are very important to specifically analyse the lithography process's reproducibility and the AZ4562 PR behaviour during the thermal reflow, i.e., during the heating above its glass transition temperature. In addition, cross-sectional diameter and sagitta are used for focal length determination, an important parameter to control according to the cylindrical ML's optical application. An optical application example, where the good reproducibility of the focal length is necessary, is the MLs array integration on top of photodiodes CMOS array to improve the light acquisition and, consequently, the current generation in each photodiode.

2. Microlenses fabrication

2.1. Geometrical parameters

In MLs with a spherical cross-section, the diameter (D) and the sagitta (h) are the two most important geometrical parameters and these are chosen according to focal length (f_0) required for a specific application. The focal length (f_0) and curvature radius (R_c) are given by:

$$f_0 = \frac{n_1}{n_2 - n_1} R_c \tag{1}$$

$$R_c = \frac{r^2 + h^2}{2h} \tag{2}$$

where n_1 and n_2 are the refractive indices of the medium and ML material for a specific wavelength, respectively. The quantities r and h are the radius and sagitta of ML, respectively. Additionally, the diameter and the height are a crucial part to control on each step of the fabrication process. Fig. 1 shows these two parameters for focal length calculation [16].

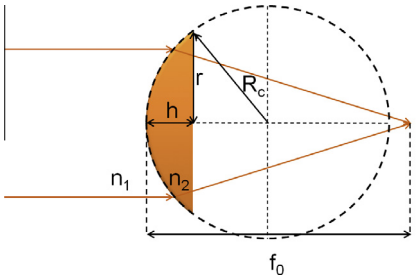

Fig. 1. MLs parameters and focal length representation.

2.2. Fabrication process

Fig. 2 represents a scheme of MLs fabrication process. Firstly, the PR (in this case a positive PR) is patterned in a glass substrate resorting to photolithography. This phase is represented in Fig. 2(a)–(c). As illustrated in Fig. 2(d), a thermal reflow process is applied in the end of photolithography for acquisition of the lens's spherical profile.

Basically, a photolithography process consists in three steps: the preparation of the sample in a substrate, the designing of a photo-mask and the pattern transfer into polymers materials by ultra-violet (UV) embossing [17]. Firstly, a PR material (polymeric materials, normally) is spun on a substrate. By controlling the speed and time of spin coating a uniform layer with a specific thickness is obtained. After, a prebake phase is necessary to remove the solvents present in the PR. Temperature and time are the parameters to control in this step. Besides removing the solvents, the prebake phase also removes the water from the PR. So a rehydration step is essential for allowing the material to absorb the water normally from the air humidity. The following phase, named exposure, includes the correct position and alignment of a photo-mask on the top of PR and the consequent exposition to UV light. This phase is dependent of the first step of photolithography: the time of exposure varies with the PR thickness, which is controlled by spin coating. A developing phase with the appropriate developer and respective concentration is required for removing the exposed PR. Finally, a three-dimensional structure correspondent to the two-dimensional photo-mask design is obtained after cleaning the samples.

The reflow method involves the melting of micro-patterned PR [3]. During the melting of PR, their liquid surfaces are pulled into a shape which minimizes the energy of the system. If gravitational effects are presumed to be negligible, which on micro-scale will generally be the case, it is expect a MLs' shape presenting a spherical surface. This occurs due to surface tension phenomenon [8,9]. Temperature and time are the parameters to control in the thermal reflow process, depending on the glass transition temperature of the PR. For AZ4562 MLs fabrication, the selected process parameters are summarized in the Table 1. The spin coating parameters were tuned to obtain a theoretical thickness of 5.06 μm. The exposure and developing parameters were readjusted in order to obtain better results. Finally, it was observed the softening point of AZ4562 to be 110 °C. However, during the fabrication optimization, it was realized that the best reflow conditions were obtained with the use

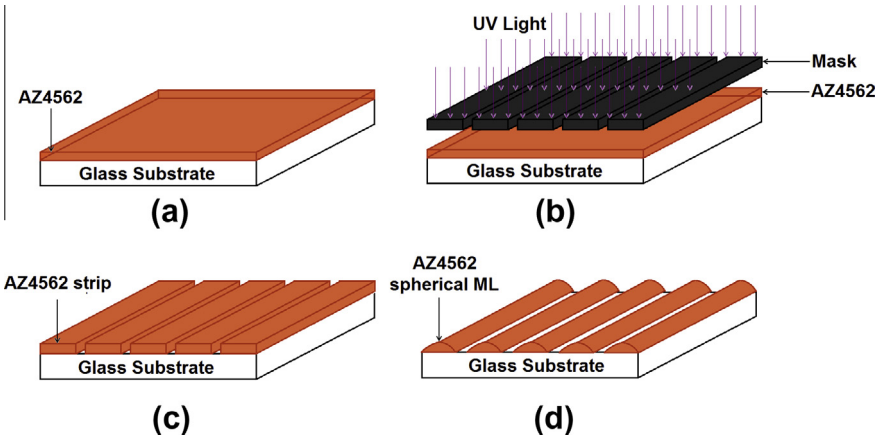

Fig. 2. MLs array fabrication steps: (a) spin coating, prebake and rehydration; (b) exposure; (c) developing and cleaning; and (d) thermal reflow.

Table 1
The MLs fabrication process steps and parameters.

Process step	Process parameters
Spin coating	20″ @ 6000 RPM[a]
Prebake	10′ @ 100 °C
Rehydration	10′ @ room temperature
Exposure	51″ @ 134 W
Developing	AZ400 K developer in a 1:4 concentration with distilled water (2′ 15″) × 2
Thermal reflow	5′ @ 140 °C

[a] RPM: revolutions per minute.

of a hotplate in a temperature of 140 °C during 5 min. Further details about the modelling of reflow and the numerical solving of Navier–Stokes equations (responsible for governing the flow of low-viscosity materials) can be found in the research done by von Lavante et al. [18].

2.3. Design specifications

As described in the previous section, the photolithography process involves a design phase of a photo-mask, which will be used for UV exposure in contact mode. This two-dimensional design is responsible to create a three-dimensional structure in PR. Therefore, in photo-mask design only the cross-sectional diameter and the distance between adjacent MLs can be controlled. Fig. 3 represents the two photo-masks used to pattern the PR in the exposure step: (a) 24 μm and (b) 30 μm strips with a spacing of 5 μm and a length of 4.9 mm. The mask of 24 μm diameter MLs has 172 strips, while the mask of 30 μm diameters MLs has 142. The height of three-dimensional structure is controlled by spin coating phase, through spin speed and time. During 20 s with a speed of 6000 RPM it is expected a height of 5.06 μm.

3. Measurement

3.1. Pre-reflow and post-reflow

Four groups of MLs arrays were fabricated for pre-reflow and post-reflow statistical analysis. Five random measurements in different strips/MLs were realized for each array, resorting to Scanning Electron Microscope (SEM) images. It was used five random measurements (an odd number) of the total array for a more significantly statistical study. The same statistical procedure was applied by Bilro et al. [19]. The micro-patterned PR and the final MLs array present a high aspect ratio, defined by ratio between the length of the array and the cross-sectional diameter of the strip/ML, i.e., the ratio L/D when L is the array's length and D is the cross-sectional diameter of a single strip or ML. The photolithographic process used for MLs' fabrication produces negligible variations in L when it is compared with the diameter D of the strips. Therefore the aspect ratio is less sensitive to small variations of the length L. On the other hand, it is extremely sensitive to the variations of D, being this one of the parameters chosen for studying. The valour of D is almost constant along L. This uniformity can be seen in Figs. 4 and 5 which represents SEM images of the strips/MLs array for the two types of MLs. Fig. 6 represents SEM images of pre-reflow measurements of two selected samples. These selected samples were randomly chosen from the entire fabricated set. Once again, Fig. 7 also shows two selected samples of MLs arrays after the thermal reflow process. The results show the spherical shape, according to theoretical concepts.

3.2. Statistical analysis

For the statistical analysis, a difference between the real and the theoretical value expected were calculated [20,21]. The expected cross-sectional diameter and distance

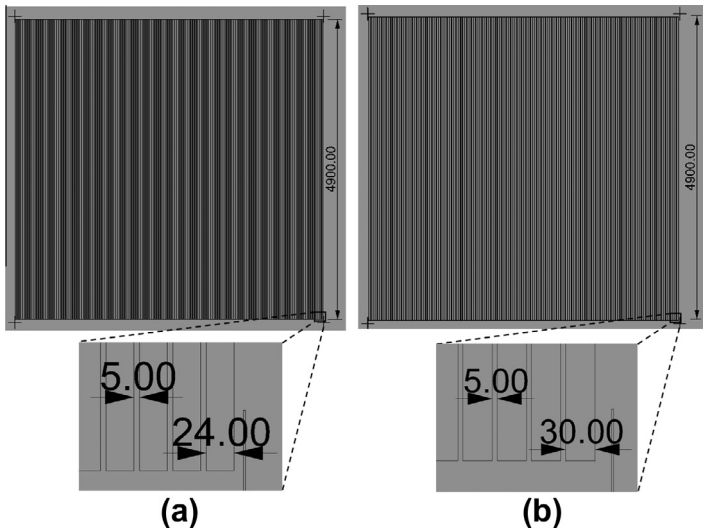

Fig. 3. Photo-masks used in MLs fabrication: (a) 24 μm diameter and (b) 30 μm diameter.

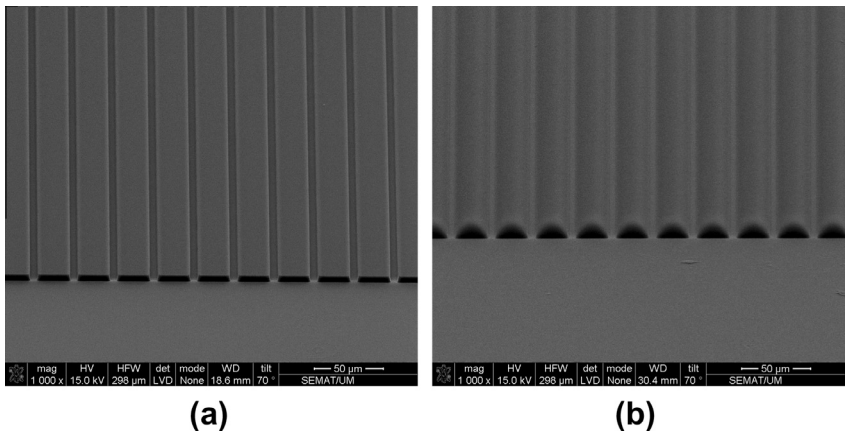

Fig. 4. For a selected sample, SEM images of 24 μm diameter array: (a) pre-reflow and (b) post-reflow.

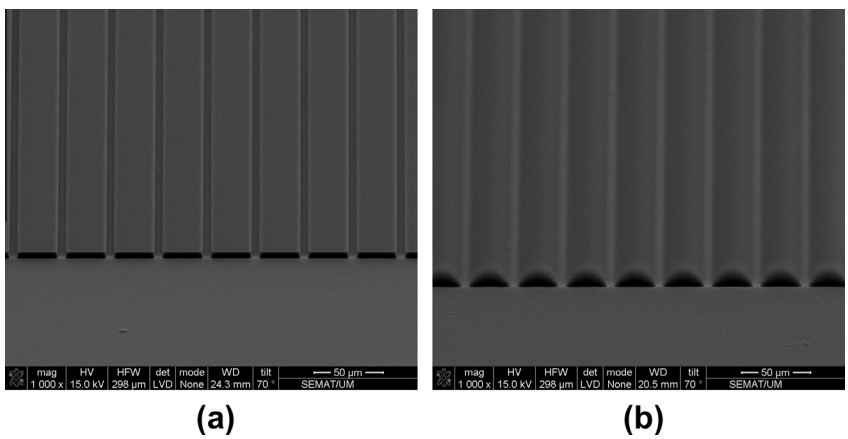

Fig. 5. For a selected sample, SEM images of 30 μm diameter array: (a) pre-reflow and (b) post-reflow.

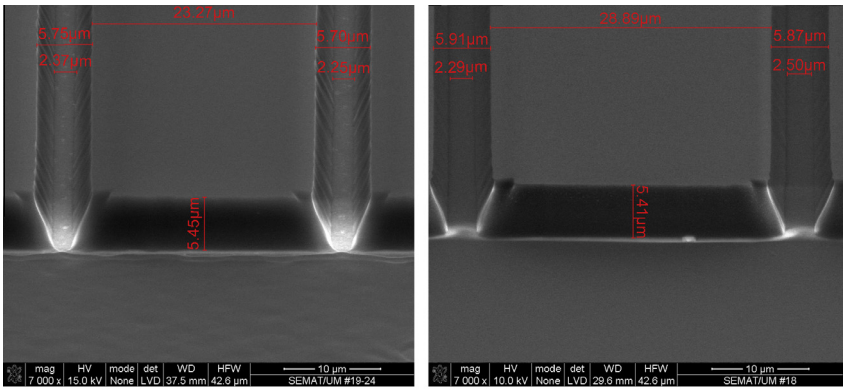

Fig. 6. For a selected sample, SEM images of pre-reflow results: (a) a single strip of a 24 µm diameter array and (b) a single strip of a 30 µm diameter array.

between adjacent MLs correspond to the photo-mask design. On the other hand, the expected MLs' sagitta is specified by the process fabrication. So, for a given parameter x, this difference is obtained by:

$$\Delta x_{i,j} = x_{i,j} - x_{th} \tag{3}$$

where $x_{i,j}$ and xth are the real and theoretical value, respectively, with $i = 1,2,3,4$ which correspond to the four groups of MLs fabricated; and $j = 1,\ldots,n$ where n is the five data collected for each group of MLs. Therefore, the mean of the difference for a parameter xth in the group i is [20]:

$$\mu_{i,x_{th}} = \frac{1}{n}\sum_{j=1}^{n}\Delta x_{i,j} \tag{4}$$

In the same way, the standard deviation (SD) is given by [17]:

$$\sigma_{i,x_{th}} = \sqrt{\frac{1}{n-1}\sum_{j=1}^{n}\left(\mu_{i,x_{th}} - \Delta x_{i,j}\right)^2} \tag{5}$$

A plot with mean *versus* SD was made for each parameter, before and after the thermal reflow. The final mean and SD, which will be used for accuracy and precision calculation, is obtained by:

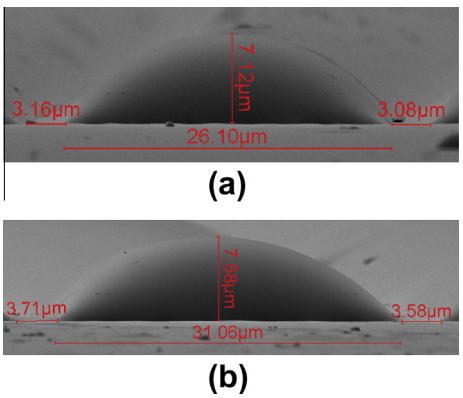

Fig. 7. For the selected samples, SEM images of post-reflow results: (a) a single element of a 24 µm diameter MLs array and (b) a single element of a 30 µm diameter MLs array.

$$S = \left(\mu_{x_{th}}, \sigma_{x_{th}}\right) = \min\sum_{i=1}^{4}\left(\mu - \mu_{i,x_{th}}\right)^2 + \left(\sigma - \sigma_{i,x_{th}}\right)^2 \tag{6}$$

This result correspond to the mean and SD that minimize the error of the differences. Finally, the accuracy and precision were calculated as follows:

$$Accuracy = \frac{\mu_{x_{th}}}{x_{th}} \times 100\% \tag{7}$$

$$Precision = \frac{\sigma_{x_{th}}}{x_{th}} \times 100\% \tag{8}$$

using the mean and SD, respectively.

3.3. Results

The following sections present the results of the statistical study and the main conclusions. For all plots, the diamonds and circle markers are the mean and SD for the four MLs groups $(\mu_{i,x_{th}}, \sigma_{i,x_{th}})$. The triangular and square markers are the final mean and SD, which result of Eq. (6). Diamonds and triangular markers are the results for 24 µm arrays, while circles and square markers refer to the 30 µm arrays' results. Firstly, the results of cross-sectional diameter study are presented. Fig. 8 represents the pre-reflow results of diameter difference for 24 and 30 µm MLs. The measurements are compared to the theoretical values expected, i.e., 24 µm or 30 µm.

On the other hand, Fig. 9 represents the pos-reflow results of diameter difference for the two MLs array. It is intended to conclude the capacity of the MLs fabrication process into transfer the photo-mask's pattern into the PR.

Table 2 resumes the main pre- and post-reflow results for the two MLs produced, in terms of diameter difference. For the 24 µm diameter mask, the fabrication process is able to produce strips with a cross-sectional diameter average of 26.78 µm with a standard deviation (SD) 0.22 µm (e.g., an average of 26.78 ± 0.22 µm of SD), before the thermal reflow. After the thermal reflow, the process produces MLs with a cross-sectional diameter average of 26.34 ± 0.35 µm of SD. This last value reflects an accuracy of 9.75% and a precision of 1.46%. Once the variable is the

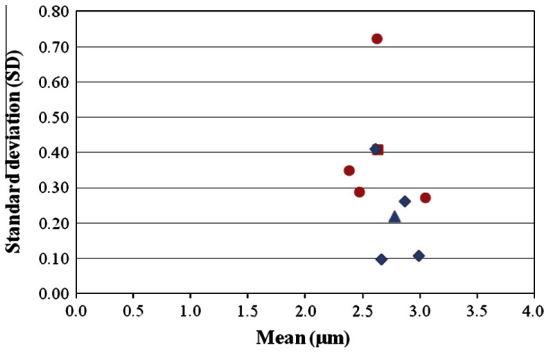

Fig. 8. Pre-reflow diameter difference for 24 μm strips (diamonds and triangular markers) and 30 μm strips (circles and square markers).

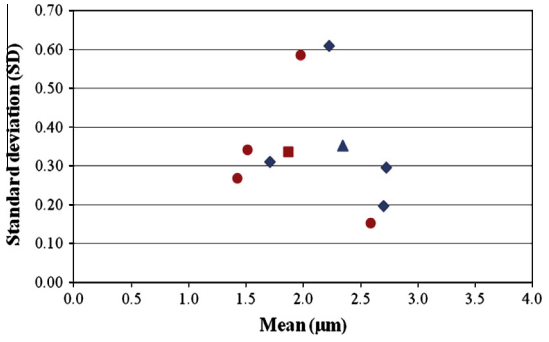

Fig. 9. Post-reflow diameter difference for 24 μm MLs array (diamonds and triangular markers) and 30 μm MLs array (circles and square markers).

difference between real and theoretical value, it's expected a small value for both the accuracy and precision.

For the 30 μm diameter mask, the fabrication process produces strips with a diameter difference of 2.64 ± 0.41 μm of SD pre-reflow. A difference of 1.87 ± 0.34 μm of SD was obtained after thermal reflow, which signify that it is obtained MLs with a cross-sectional diameter average of 31.87 μm post-reflow. The reproducibility of 30 μm MLs array fabrication corresponds to an accuracy of 6.23% and a precision of 1.13%.

To a complete study of the photo-mask's pattern transference into the PR, during the exposure phase, a statistical study of distance between adjacent MLs was made, comparatively to the theoretical value of 5 μm expected for the two arrays. For the two arrays, Figs. 10 and 11 represent the pre-reflow and post-reflow results, respectively.

Table 3 presents the main results of the distance between adjacent MLs study. It is possible to observe that

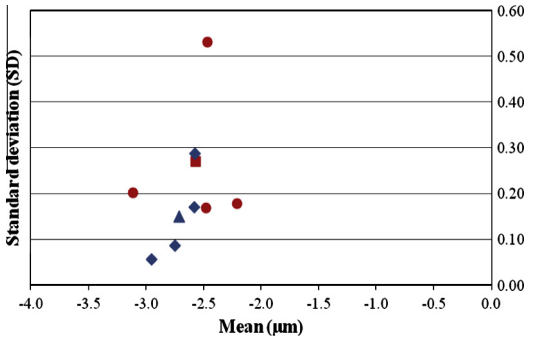

Fig. 10. Pre-reflow distance difference between adjacent lenses for 24 μm diameter strips (diamonds and triangular markers) and 30 μm diameter strips (circles and square markers).

the distance is smaller than the theoretical value of 5 μm. This general result is in accordance with the diameter study, i.e., the increase of the diameter from the mask to the PR is compensated by the decrease of the distance between adjacent MLs. For 24 μm diameter mask, the mean difference of the distance obtained was −2.71 ± 0.15 μm of SD before reflow. For 30 μm strips, a mean difference of −2.57 ± 0.27 μm of SD before thermal reflow was obtained. On post reflow phase, the distance between adjacent lenses increases, according to the decrease of diameter verified with the thermal reflow. A mean difference of −2.21 ± 0.29 μm of SD and of −1.87 ± 0.30 μm of SD was obtained for 24 μm and 30 μm MLs array after the reflow.

Finally, a study of MLs' sagitta was made. This study was based in the difference between real value measured in SEM images and the theoretical value expected by spin coating parameters: 5.06 μm. Figs. 12 and 13 represent the pre-reflow and post-reflow height difference results, respectively.

The mean of height difference increases from pre-reflow to post-reflow phase. This can be consulted in Table 4. So the height increases with the thermal reflow process due to the melting of PR. An average height difference of 0.76 ± 0.10 μm of SD and of 0.71 ± 0.12 μm of SD was obtained for 24 μm and 30 μm micro patterned strips, before the thermal reflow. In this phase the difference is very low, which means that the photolithography process reproduces approximately the thickness expected. However, after the thermal reflow, this difference increases to 1.91 ± 0.15 μm of SD and to 2.24 ± 0.24 μm of SD for 24 μm and 30 μm MLs array, respectively. With the height study is possible to conclude that the SD, generally, is smaller than the other parameters (diameter and distance between adjacent lenses difference). This corresponds to a

Table 2
Mean and standard deviation of diameter difference pre- and post-reflow.

MLs array (μm)	Phase	Mean (μm)	Accuracy (%)	Standard deviation (μm)	Precision (%)
24	Pre-reflow	2.78	–	0.22	–
	Post-reflow	2.34	9.75	0.35	1.46
30	Pre-reflow	2.64	–	0.41	–
	Post-reflow	1.87	6.23	0.34	1.13

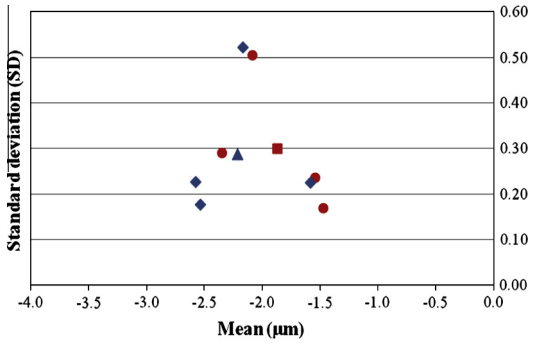

Fig. 11. Post-reflow distance difference between adjacent lenses for 24 μm MLs array (diamonds and triangular markers) and 30 μm MLs array (circles and square markers).

Table 3
Mean and standard deviation of distance difference between adjacent lenses pre- and post-reflow.

MLs array (μm)	Phase	Mean (μm)	Standard deviation (μm)
24	Pre-reflow	−2.71	0.15
	Post-reflow	−2.21	0.29
30	Pre-reflow	−2.57	0.27
	Post-reflow	−1.87	0.30

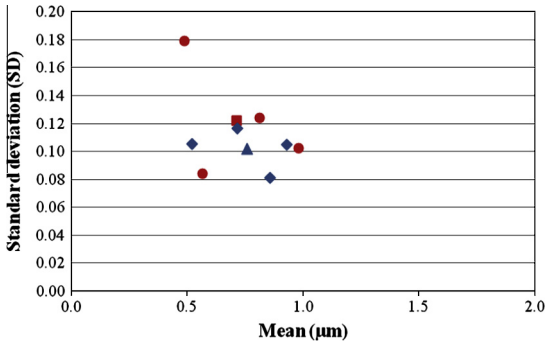

Fig. 12. Pre-reflow height difference for 24 μm diameter strips (diamonds and triangular markers) and 30 μm diameter strips (circles and square markers).

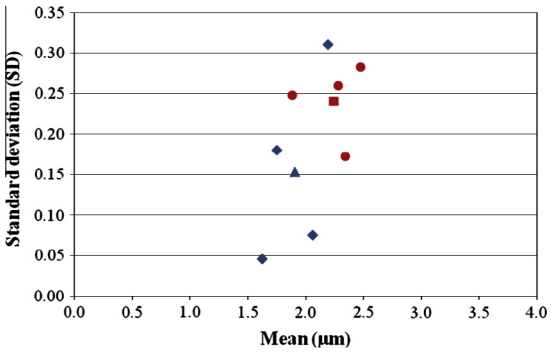

Fig. 13. Post-reflow sagitta difference for 24 μm MLs array (diamonds and triangular markers) and 30 μm MLs array (circles and square markers).

Table 4
Mean and standard deviation of height difference pre- and post-reflow.

MLs array (μm)	Phase	Mean (μm)	Accuracy (%)	Standard deviation (μm)	Precision (%)
24	Pre-reflow	0.76	–	0.10	–
	Post-reflow	1.91	7.96	0.15	0.63
30	Pre-reflow	0.71	–	0.12	–
	Post-reflow	2.24	7.47	0.24	0.80

better precision. Thus, for the total fabrication process, a precision of 0.63% and 0.80% was obtained for 24 μm and 30 μm arrays, respectively. An accuracy of 7.96% and 7.47% was obtained for the same arrays, respectively.

4. Conclusion

This paper presented a fabrication process of MLs based on photolithography and thermal reflow. A statistical validation of the same was made. This successful validation concluded the correct transfer of the photo-mask design into the AZ4562 positive PR and the proximity of the diameter and height relatively to the theoretical values. This simple, fast and low cost fabrication process presents a high degree of reproducibility for the parameters studied, opening good perspectives for applying this process in high-volume productions of MLs arrays.

Acknowledgments

This work was fully supported by the Portuguese Foundation for Science and Technology under the project FCT/PTDC/EEA-ELC/109936/2009. The authors would also like to acknowledge Dr. Ing Christian Koch from MicroChemicals GmbH for the technical support.

References

[1] V. Backmutsky, G. Vaisman, New mechatronic scanners for graphical data acquisition, conversion and representation, Measurement 23 (1) (1998) 55–62.
[2] A. Cantatore, A. Cigada, R. Sala, E. Zappa, Hyperbolic tangent algorithm for periodic effect cancellation in sub-pixel resolution edge displacement measurement, Measurement 42 (8) (2009) 1226–1232.
[3] M. Engin, A. Demirel, E.Z. Engin, M. Fedakar, Recent developments and trends in biomedical sensors, Measurement 37 (2) (2005) 173–188.
[4] J. Ponmozhi, C. Frias, T. Marques, O. Frazão, Smart sensors/actuators for biomedical applications: review, Measurement 45 (7) (2012) 1675–1688.
[5] T. Pfeifer, R. Freudenberg, G. Dussler, B.B. Brocher, Quality control and process observation for the micro assembly process, Measurement 30 (2001) 1–18.
[6] C.F. Cheung, K. Hu, X.Q. Jiang, L.B. Kong, Characterization of surface defects in fast tool servo machining of microlens array using a pattern recognition and analysis method, Measurement 43 (9) (2010) 1240–1249.
[7] S.-K. Lee, M.-G. Kim, K.-W. Jo, S.-M. Shin, J.-H. Lee, A glass reflowed microlens array on a Si substrate with rectangular through-holes, J. Opt. A: Pure Appl. Opt. 10 (4) (2008) 1–8.
[8] F.T. O'Neill, J.T. Sheridan, Photoresist reflow method of microlens production. Part I: Background and experiments, Opt. – Int. J. Light Elect. Opt. 113 (9) (2002) 391–404.
[9] P. Nussbaum, Design, fabrication and testing of microlens arrays for sensors and microsystems, Pure Appl. Opt. 6 (2000) 617–636.

[10] G.A. Cirino, S.A. Lopera, A.N. Montagnoli, R.D. Mansano, L.G. Neto, Microlens array fabricated by gray-scale lithography maskless system, ECS Trans. 49 (2012) 339–345.
[11] H.-T. Hsieh, V. Lin, J.-L. Hsieh, G.-D.J. Su, Design and fabrication of long focal length microlens arrays, Opt. Commun. 284 (21) (2011) 5225–5230.
[12] V. Lin, H.-C. Wei, H.-T. Hsieh, J.-L. Hsieh, G.-D.J. Su, Design and fabrication of long-focal-length microlens arrays for Shack–Hartmann wavefront sensors, Micro Nano Lett. IET 6 (7) (2011) 523–526.
[13] E. Roy, B. Voisin, J.-F. Gravel, R. Peytavi, D. Boudreau, T. Veres, Microlens array fabrication by enhanced thermal reflow process: towards efficient collection of fluorescence light from microarrays, Microelectron. Eng. 86 (11) (2009) 2255–2261.
[14] S. Audran, B. Mortini, B. Faure, G. Schlatter, Dynamical formation of microlenses by the reflow method: numerical simulation and experimental study of the process fabrication, J. Micromech. Microeng. 20 (9) (2010) 1–9.
[15] M. Kim, T. Scharf, H.P. Herzig, Small-size microlens characterization by multiwavelength high-resolution interference microscopy, Opt. Express 18 (14) (2010) 14319–14329.
[16] D. Daly, R.F. Stevens, M.C. Hutley, N. Davies, The manufacture of microlenses by melting photoresist, Meas. Sci. Technol. 759 (1990).
[17] H.-H. Kim, B.-H. O, S.-G. Lee, S.-G. Park, Fabrication of novel double microlens using two step soft lithography, Microelectron. Eng. 87 (5–8) (2010) 1033–1036.
[18] E. von Lavante, A. Zachcial, B. Nath, H. Dietrich, Unsteady effects in critical nozzles used for flow metering, Measurement 29 (1) (2001) 1–10.
[19] L. Bilro, J.G. Oliveira, J.L. Pinto, R.N. Nogueira, A reliable low-cost wireless and wearable gait monitoring system based on a plastic optical fibre sensor, Meas Sci Technol 22 (4) (2011) 045801.
[20] M. Wang, D. Han, S. Li, The application and research of high-frequency ultrasonic reflection technique used in the measurement of small diameter's tube cavity size, Measurement 46 (1) (2013) 521–526.
[21] J.P. Carmo, J. Antunes, M.F. Silva, J.F. Ribeiro, L.M. Goncalves, J.H. Correia, Characterization of thermoelectric generators by measuring the load-dependence behavior, Measurement 44 (10) (2011) 2194–2199.